Current Blockade in Nanopores in the Presence of Double-Stranded DNA and the Microscopic Mechanisms

Shengting Cui

Department of Chemical and Biomolecular Engineering, University of Tennessee, Knoxville, Tennessee 37996-2200

Received: October 6, 2009; Revised Manuscript Received: November 18, 2009

We have carried out Brownian Dynamics calculations to investigate the mechanism of current blockade by double-stranded DNA (dsDNA) in a nanopore. We find that the blockade current crosses over from negative to positive as the ionic concentration decreases, similar to experiment. In addition to the volume exclusion and the counterion condensation, we find that the electric double layer overlap is a significant factor in the current blockade. The electric double layer overlap causes the ionic concentration beyond the immediate neighborhood of dsDNA and the wall to be lower in a dsDNA-blocked nanopore than the plateau ionic concentration away from the wall in an open nanopore, thus contributing importantly to the blockade current. On the basis of the calculated ion distribution function in the nanopore, we examined the counterion condensation to the dsDNA. We find the excess counterion condensation to be about 60% of the charge on the dsDNA, which is within the range of percentages obtained from experiments. We performed equilibrium and nonequilibrium (under an applied electric field) Brownian dynamics simulations to calculate the average mobility of the ions in nanopores. The calculated ion mobility is found to be reduced in DNA-blocked nanopores.

I. Introduction

Detection of DNA-induced ionic current blockade has attracted considerable recent interest[1–9] as nanopores with diameter on the scale of ~10 nm and smaller have been constructed. Several recent works have reported observing the current blockade crossing from being negative to positive as the ionic concentration is reduced.[5–9] Simple analyses based on the concepts of volume exclusion and counterion condensation on DNA have provided reasonable interpretation of the crossover phenomenon. Some inconsistencies, however, still exist. For example, using different sized nanopores, experiments in refs 5 and 6 obtained different crossover concentrations. In rationalizing their results, different counterion condensation fractional numbers were used to obtain crossover concentrations consistent with their respective experiments. Alternatively, it is possible that other mechanisms may also be in operation in ionic current conduction in nanopores. A full understanding of these effects would be useful for interpreting and correlating experimental results as increasingly smaller nanopores are being constructed for such applications. One such mechanism is the electric double layer (EDL) overlap effect,[10,11] which causes the co-ions to be more strongly excluded, whereas the counterions are enriched[12] (assuming the nanopore carries negative charge). Introduction of a highly charged DNA inserts an additional EDL into the nanopore and thus enhances the EDL overlap, leading to a significant difference in the ionic concentration in the nanopore in the presence of DNA compared to that in its absence. Furthermore, DNA conformation also plays a role, one direct consequence of which is the increase of electric charges carried by the DNA as the contour length of the double-stranded DNA (dsDNA) is longer than the length of the nanopore.[13,14] Significant interest also exists in the counterion condensation to the DNA,[15] and a number of experiments have been conducted to obtain the amount of counterion condensation onto DNA. However, divergent values have been given on the amount of counterion condensation, perhaps depending on the experimental techniques used, as well as the types of the counterion (such as valence and size), ranging from 0.53−0.85 in terms of the fraction of dsDNA charge being neutralized by the counterion.[15–20]

We conducted a Brownian dynamics simulation study to obtain a detailed understanding of the microscopic mechanisms for ionic current conduction in nanopores. For this goal, we studied two aspects of the system that are relevant to the current conduction: (1) the equilibrium partition of ions between DNA-blocked and open nanopores, and (2) the migration mobility of ions in nanopores. We calculated and carried out detailed analysis of ion distributions around DNA in the nanopore to examine the effects such as EDL overlap and counterion condensation to gain insight into the ionic behaviors. Our calculations were carried out for a nanopore 10 nm in diameter, corresponding to the nanopore sizes used in recent experiments,[6] so that comparison can be made. In the following, we present our methods and results. We discuss the results to elucidate our understanding of the microscopic mechanisms of current blockade in nanopores.

II. Models and Methods

We carried out the Brownian dynamics study of DNA in nanopores with K^+ and Cl^- ions for a range of concentrations. The geometry of the system is shown schematically in Figure 1. The nanopore consists of two subregions. One region contains a segment of dsDNA (DNA region); the other contains no DNA (which we refer to as the buffer pore region throughout the paper). In the theory of ionic solutions,[10,11] the extent of the effect by a charged wall is characterized by the Debye length, which is given (in SI units) by $\lambda_D = (k_B T\varepsilon/e^2 c_s)^{1/2}$ for monovalent ionic solution, where k_B is the Boltzmann constant, T is

10.1021/jp909564d
Published on Web 01/13/2010

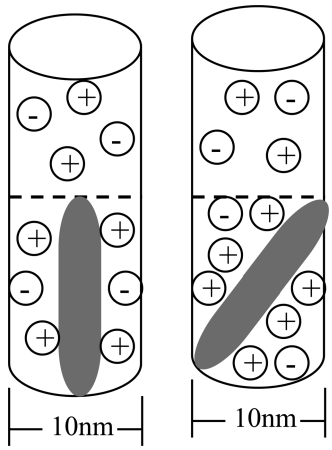

Figure 1. Schematics of the simulation system. The figure on the left illustrates a dsDNA placed at the radial center of a nanopore with the axis of the dsDNA parallel to that of the nanopore. The figure on the right illustrates that the DNA is tilted to form an angle with the nanopore axis. The ends of the dsDNA are capped with semispheres. Approximately half of the pore is occupied with dsDNA, and the remainder is open.

temperature, ε is the dielectric constant, e is the magnitude of electron charge, and c_s is the total number density of the ions. Using the expression, we can estimate that, for ionic concentration at 0.01 M, which is the smallest ionic concentration studied here, the Debye length is about 3.04 nm, which is less than the radius of the nanopore (5 nm) used in this study. Thus, in the buffer pore region, sufficiently far from the wall, the ion concentration can be reasonably assumed to be equal to that of a bulk reservoir. For ionic concentration lower than 0.01 M, the Debye length becomes equal to or exceeds the nanopore radius, and this assumption becomes invalid.

When equilibrium is established between the two regions, the ions appropriately partition between them so we can obtain the number of ions (or concentrations) in each region. When the migration mobilities of the ions in the nanopore are known, we can calculate the current flow through the nanopores with and without DNA and then the current difference to determine the blockade current due to the presence of DNA in the nanopore.

In our system, the dsDNA is fixed in space. Only ions undergo Brownian motion. The equation of motion for the ions is[21,22]

$$m_i \frac{d\mathbf{v}_i}{dt} = \mathbf{f}_i - \varsigma_i \mathbf{v}_i + \mathbf{f}_i^R \qquad (1)$$

where m_i is the mass of the ion (labeled with index i), $\mathbf{v}_i$ is the instantaneous velocity vector, $\varsigma_i = k_B T/m_i D_i$ is the friction coefficient, with D_i being the self-diffusion coefficient, k_B being the Boltzmann constant, and T being the temperature. $\mathbf{f}_i$ is the force due to other ions, DNA, the pore, and the applied field, and $\mathbf{f}_i^R$ is the random Brownian force representing the effect of the solvent. The position and velocity are updated using the standard algorithm.[23] The main reason that the DNA can be treated as immobile is because it moves much slower than the ions. At a temperature of 298 K, K^+ has a thermal velocity of about 436 m/s, and that for Cl^- is slightly faster. The thermal velocity of DNA, on the other hand, is much slower. Considering a DNA segment equal to its persistent length, ~50 nm, for example, its thermal velocity would be about 13 m/s, more than an order of magnitude slower than that of an ion. In practice, DNA lengths used in typical experiments are hundreds of times longer than its persistent length, thus its thermal motion is negligible compared to that of the ions.

In our calculations, the DNA is modeled as a straight cylinder, with an exclusive core radius 0.80 nm, and negative charges of $-e$ each are placed 0.3 nm out from the core surface in double-helical arrangement. The DNA is capped with hemispherical caps of 0.80 nm at both ends.[24] The total length of the pore in most calculations is 21.76 nm in length (longer for low ion concentration), and 10 nm in diameter. Approximately half of the pore length is occupied with the DNA, the rest is the buffer pore with only ions. The length of the DNA is different depending on whether the DNA is parallel to the cylindrical axis or tilts with an angle. We studied two cases: one in which the DNA is at the center of the pore and parallel to the axis of the pore; the other in which the DNA forms an angle with the pore axis to model a straight short segment of a long flexible dsDNA. The DNA lengths considered here (less than 13 nm) are less than the persistence length of the dsDNA (~50 nm), and are aimed to represent a short segment of a long dsDNA, which should be reasonably straight and randomly oriented in a nanopore within the limiting maximum angle. In this initial study, we have chosen to allow the DNA to assume the maximum angle allowable within the geometry of the nanopore, ~35.6°. In the case when the DNA is parallel to the axis, the total length of the DNA (including the hemispherical caps) is about 10.7 nm and carries 50 negative electric charges. For the DNA tilted, the total length is 12.7 nm and carries 62 negative electric charges. The K^+ and Cl^- interact with the DNA and with each other through a soft sphere potential and electrostatic interaction.[25] The dielectric constant of the media is 78.4, modeling the aqueous environment. The interaction models and the pertinent parameters relevant in this study are summarized in Table 1 for a clear reference.

Before proceeding further, we briefly comment on the efficacy of the simple model for DNA used here. The current conduction in nanopore in the presence of DNA is essentially an electrokinetic phenomenon (ion motion and distribution) of the small ions, which is dominated by the electrostatic interaction between the ions and the DNA. The role of the volume exclusion is straightforward and is modeled here by a cylindrical volume because the DNA is relatively stiff with a persistent length of about 50 nm, which is much larger than the size of the ions (~0.4 nm). The most important is to properly represent the electrostatic interaction. At the fundamental level, this is rooted in the fact that the electrostatic interaction in aqueous solution is about an order of magnitude stronger than the typical van der Waals interaction at close contact for small ions. This is why coarse-grained mean field approaches such as the Poisson−Boltzmann theory for treating ionic solution have been successful and widely used.[10,11] The most prominent features for the DNA compared to other nonbiological cylindrical bodies, such as a silica cylinder, are its high charge density and the helical arrangement of the charges. The model we used here captures these most important characteristics of DNA so it can reproduce the main features of the phenomenon. The electrostatic interaction is also long-ranged (theoretically with a range of infinity), and thus responsible for the EDL effect, whereas the van der Waals interaction is significant within only a few atomic diameters. With this simplified model, however, many biological functions of DNA that depend on atomic details such as sequence-specific recognition cannot be studied. However, some of the biological phenomena such as DNA wrapping around histone proteins and chromatin condensation have been

TABLE 1: Potential Models and Parameters Used in the Simulation[a]

interaction pair	ε (kCal mol^{-1})	σ (Å)	q (e)	D (10^{-5} cm^2/s)	μ (10^{-4} cm^2/V s)
K^{+b}	0.1000	3.332	+1	1.96	7.616
Cl^{-b}	0.1000	4.400	−1	2.03	7.909
K^+-wall[c]	0.1520	3.166			
Cl^--wall[c]	0.1520	3.700			
DNA charge sites[d]	0.1520	3.200			
DNA core[e,f]	0.1520	3.200			

[a] ε and σ are the Lennard-Jones energy and size parameters, q is electric charge, D is the self-diffusion coefficient, and μ is the mobility. [b] Ion−ion interaction: WCA potential: $V(r) = 4\varepsilon\{[(\sigma/r)^{12} - (\sigma/r)^6] - [(\sigma/rcut)^{12} - (\sigma/rcut)^6]\}$; Lorentz−Berthelot combining rule is used for cross interaction. [c] Ion−wall interaction: $V(r) = 4\varepsilon(\sigma/r)^{12}$, $r = (R - \rho)$; R is pore radius, ρ is radial distance of the ion. [d] Ion−DNA charge site interaction: WCA potential; Lorentz−Berthelot combining rule for the interaction. [e] Ion−DNA core interaction (cylindrical portion): $V(r) = \varepsilon(\sigma/r)^{12}$, $r = \rho - r_0$, ρ is radial distance of the ions from the DNA center axis, and $r_0 = 8$ Å is the core radius of the DNA. [f] Ion−DNA core interaction (caps): $V(\rho) = \varepsilon(\sigma/\rho)^{12}$, $\rho = |\mathbf{r}| - r_0$, $\mathbf{r} = \mathbf{r}' - \mathbf{r}_\pm$, $\mathbf{r}'$ and $\mathbf{r}_\pm$ are the position of the ion and the centers of the semispherical end-caps of the DNA, ρ is the distance from the cap surface to the ion.

TABLE 2: Partition of Ions between the DNA-Blocked Region and Buffer Pore Region of the Nanopore[a]

conc. (M)	total length (nm)	region 1 length (nm)	region 1 number of K^+	region 1 number of Cl^-	region 2 length (nm)	region 2 number of K^+	region 2 number of Cl^-
0.01	130.56	65.10	712	0	65.46	379	13
0.02	65.28	32.46	343	0	32.82	203	14
0.06	21.76	10.70	110	7	11.06	80	15
0.18	21.76	10.70	122	16	11.06	106	44
0.25	21.76	10.70	153	47	11.06	147	85
0.37	21.76	10.70	197	91	11.06	205	143
0.50	21.76	10.70	247	141	11.06	277	215
0.64	21.76	10.70	289	182	11.06	319	258
0.79	21.76	10.70	358	252	11.06	410	348

[a] Results are for DNA in the center and parallel to the axis of the nanopore at constant wall charge density.

TABLE 3: Partition of Ions between the DNA-Blocked Region and Buffer Pore Region of the Nanopore[a]

conc. (M)	total length (nm)	region 1 length (nm)	region 1 number of K^+	region 1 number of Cl^-	region 2 length (nm)	region 2 number of K^+	region 2 number of Cl^-
0.06	21.76	10.77	122	6	10.99	80	16
0.18	21.76	10.77	136	21	10.99	103	39
0.25	21.76	10.77	167	49	10.99	145	83
0.37	21.76	10.77	210	92	10.99	204	142
0.50	21.76	10.77	265	147	10.99	271	209
0.64	21.76	10.77	296	178	10.99	324	262
0.79	21.76	10.77	377	258	10.99	403	342

[a] Results are for DNA tilted at an angle of 35.6° with the axis of the nanopore at constant wall charge density.

shown to be electrostatically driven, and have been studied using similar coarse-grained models. Interested readers are referred to ref 26 for further reading on the subject.

The wall of the pore is modeled as carrying uniformly distributed negative charges. Discrete charges of $-e$ are embedded on the wall at radial position 5 nm, in a ring-like fashion at a 120° angle apart. The charge sites of neighboring rings are rotated by 60° from each other to more uniformly disperse the charges on the wall surface. In one case we studied, the wall charge density is kept constant at 27.6 mC/m^2 at all ionic concentration,s approximately corresponding to a silica surface at high ionic concentration.[6,27,28] In the other case, the wall charge density is allowed to vary in accordance to the silica surface charge density.[27,28] The time step used for updating the position and velocity of the ions is 0.0336 ps. Typical calculations run for 5−10 million time steps, in the range of 168−336 ns.

The electrostatic long-range interaction is treated as in our previous publication.[29] Because of the one-dimensional nature of the system at large distances and the electric neutrality of the system, the long-range correction to the electrostatic interaction can be integrated to give an analytic expression in the line-charge method approach.[30]

III. Results

III.1. Partition of Ions between the DNA and Buffer Pore Region in the Nanopore. In Tables 2 and 3, we summarize the calculated numbers of ions distributed between the two regions. Comparison between the two regions shows that, at high ionic concentration, the buffer pore region has a higher total number of ions (counterions plus co-ions) than the DNA region, suggesting the important contribution by the excluded volume effect. As the ion concentration decreases, the total number of ions in the DNA region eventually exceeds that in the buffer pore region. In addition, it is seen that, in the DNA region, the number of co-ions is significantly smaller than that of counterions, which is obviously a result of the electrostatic repulsion (co-ion)/attraction (counterion) by the DNA. The number of co-ions in the DNA region is also generally smaller than that in the buffer pore region as a result of the enhanced exclusion effect by the negatively charged DNA. The co-ion reduction becomes stronger as the ion concentration decreases, as the EDL overlap becomes stronger due to reduced screening. Below a certain concentration, around about 0.02 M, the co-ions are completely excluded by the DNA and the wall charge. Only counterions are present in the DNA region.

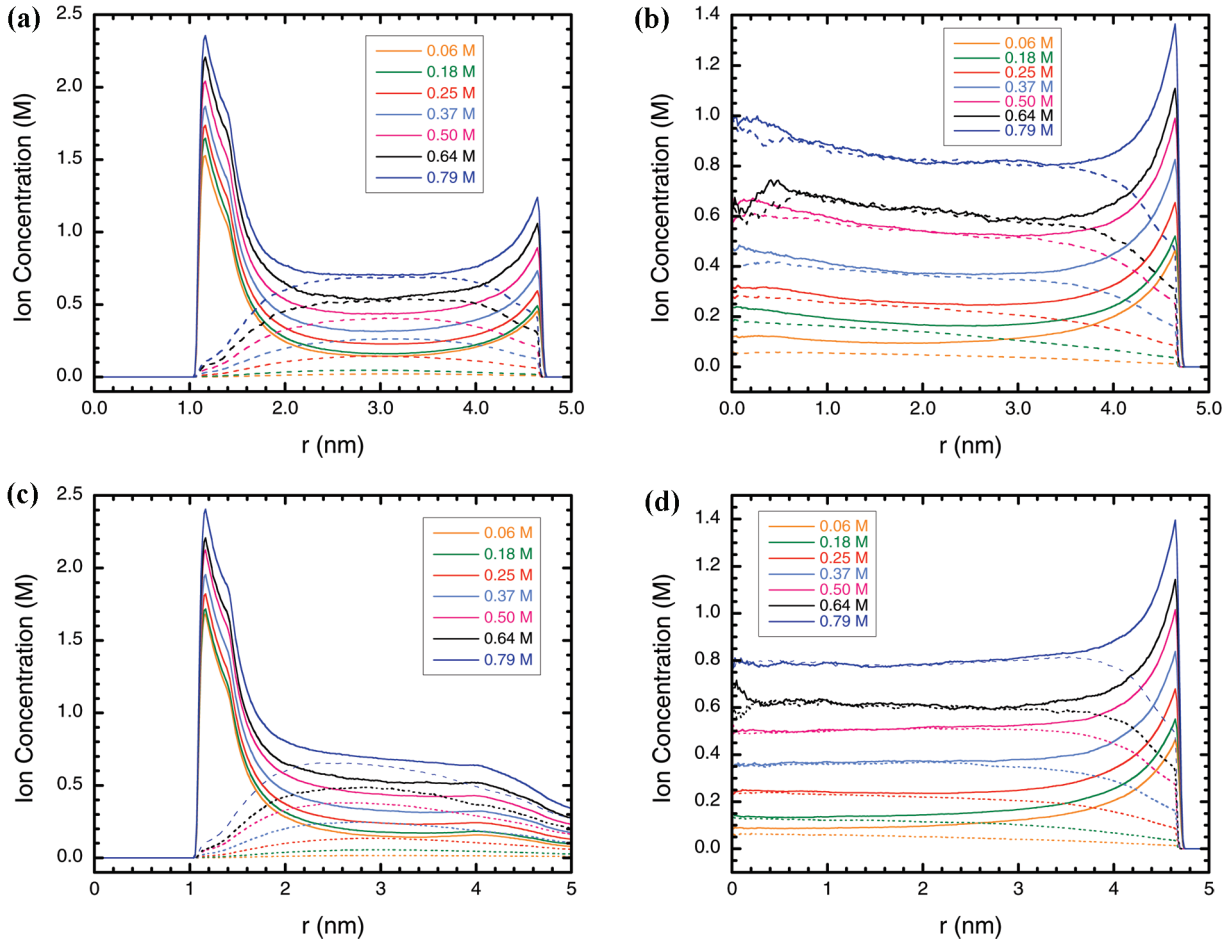

Figure 2. Ion distributions around the DNA in a blocked nanopore; and in a buffer nanopore. Solid lines are for the counterion distributions, and the dashed lines are for the co-ion distributions. (a) DNA-blocked region: DNA is centered and parallel to the nanopore axis, r is the radial distance from the axis of the DNA, which coincides with the center of the nanopore; (b) buffer pore region: DNA is centered and parallel to nanopore axis, r is the radial distance from the axis of the pore; (c) DNA-blocked region: DNA is tilted with an angle of 35.6° with respect to the pore axis, r is the radial distance from the axis of the DNA; (d) buffer pore region: DNA is tilted with an angle of 35.6° with respect to the pore axis, r is the radial distance from the axis of the pore.

III.2. Ion Distributions around DNA and in the Nanopore. To obtain a detailed picture of the ionic behavior in the presence of DNA in the nanopore, we calculated the ion distributions in the DNA region and the buffer pore region. Figure 2a,b shows the results for the case of DNA centered in the nanopore and parallel to the pore axis for a range of ion concentration. Figure 2a displays the ion distribution for the DNA region (note that the distribution function is calculated for the DNA segment containing the charges, i.e., excluding the two end-cap regions), and Figure 2b displays that for the buffer pore region. Since the DNA is centered and parallel to the pore axis, the system is cylindrically symmetric. We see from Figure 2a that, when DNA is present, the counterion distribution function shows a peak near the DNA and a peak near the wall, and a plateau region in between, with the plateau height that decreases with decreasing ion concentration. The peaks are due to the enrichment of counterions near the negatively charged sites on the DNA or the wall. The co-ion distribution, on the other hand, displays depletion near the DNA and the wall. In addition, the counterion and co-ion distribution functions become increasingly more separated as ion concentration (and the electrostatic screening) decreases, as a result of the combined effect of the negative charges on the DNA and the wall, i.e., the EDL overlap. Without the DNA in Figure 2b, the distribution function displays a peak near the wall and a more or less plateau density distribution in the interior. The slight increase near the center ($r = 0$) is due either to the DNA end-cap effect, the residual effect of the centered DNA, or both (compare to Figure 2d below where the DNA is tilted so the end-caps are near the wall). The deviation of the absolute number of ions from a flat profile, however, is very small, as the total volume within small radius in cylindrical volume is quadratically dependent on the radius (equivalent to about three ions, for example, at a concentration of 0.37 M).

Figure 2c,d shows the ion distributions for the case where DNA is tilted with respect to the pore axis with a 35.6° angle. The distributions in Figure 2c are along the radial distance from the symmetry axis of the DNA (not the pore axis). The ion distribution around DNA in this case, however, is not cylindrically symmetric and may also vary along the DNA axis near the ends. The plots in Figure 2c are results after averaging over the azimuthal angle and the axial direction of the DNA. Near the DNA, the ion distributions are similar to those in Figure 2a, because at very short distance, the ion distributions are not severely perturbed by the wall of the nanopore. At larger distance, the wall effect and the azimuthal anisotropy start to distort the ion distribution. The peak near the wall essentially disappears because it is spread out over a range of distance in the DNA-based coordinate. It is also noted that, for DNA tilted, the counterion and co-ion distribution functions shown in Figure 2c exhibit split for all concentrations studied here, even for the highest concentration 0.79 M (compare with Figure 2a). This is because the end-portion of the DNA is very near the wall.

Beyond the immediate vicinity of the DNA, the EDLs of this portion of the DNA and the wall strongly overlap, resulting in a severe distortion of the surrounding ionic cloud, causing the distribution split.

Figure 2d shows the distribution functions for the buffer pore region and is therefore plotted along the radial direction of the pore. The interior region of the distribution functions is flat as they are little affected by the DNA end-caps (which are in this case near the wall). The plateau interior density of the ions also provides a reasonable estimate of the ionic concentration at which equilibrium with bulk reservoir is established. At ionic concentration equal to and above 0.18 M, positive and negative ion profiles coincide near the center so this common concentration is taken to represent the bulk concentration. At ionic concentration somewhere between 0.18 and 0.06 M and lower, the positive and negative ion profiles start to split. In this case, we have taken the co-ion concentration near the center as an approximation to the bulk concentration. This may slightly underestimate the bulk concentration with which it is in equilibrium. But since the concentration is low, the absolute error should be small. In particular, this should not affect the determination of the crossover concentration for the blockade current, as it occurs at relatively high ionic concentration (above 0.18 M; see section III.5 below). Comparison of the ion distributions also shows that the plateau region of the ion distribution in the presence of DNA is lower than those in the absence of DNA. This again points to the EDL overlap effect where the stronger repulsion by negatively charged DNA and wall charges push out the co-ions. Electric neutrality then operates to reduce the number of counterions accordingly.

The EDL overlap in the presence of DNA can significantly affect the amount of ions in the nanopore and, in turn, the blockade current. To illustrate, we show in Figure 3a,b the ionic number difference within a radial distance between region with DNA and the region without DNA for a range of concentration for the case where the DNA is centered and parallel to the pore axis. This is obtained by calculating the number of each type of ions within a certain radial distance by integrating over the radial distribution functions and multiplying by the length of each region and then taking the difference. Figure 3a shows the results for the counterion and co-ion separately, and Figure 3b shows the sum of the two. As seen from the figures, for r less than about 1.1 nm, the excess charges for counterion, co-ion, and total all decrease as a result of the excluded volume effect. Then as r increases, the excess counterion increases due to the counterion condensation effect either reach a maximum and then continuously decrease to the wall, or continue to increase slightly (for ionic concentrations less than about 0.06 M); whereas the co-ion excess charge monotonically decreases over the entire radial distance as a result of the EDL overlap effect. The total excess charge follows roughly the same trend as the counterion but reaches maximum at a slightly different radial distance depending on the rate of decrease in the contribution by the co-ion. The continuous variation (downward for high and moderate ion concentration) in the excess charge beyond the condensation layer of the counterion to the DNA suggests that the EDL overlap has a significant effect on the ionic current and in turn the crossover concentration for the blockade current. Without the EDL overlap effect, the plots in Figure 3a,b would be flat beyond the counterion condensation layer.

III.3. Counterion Condensation to the DNA. It is noted in Figure 2a,c that counterions accumulate near the DNA to neutralize the charge of the DNA, as demonstrated by the

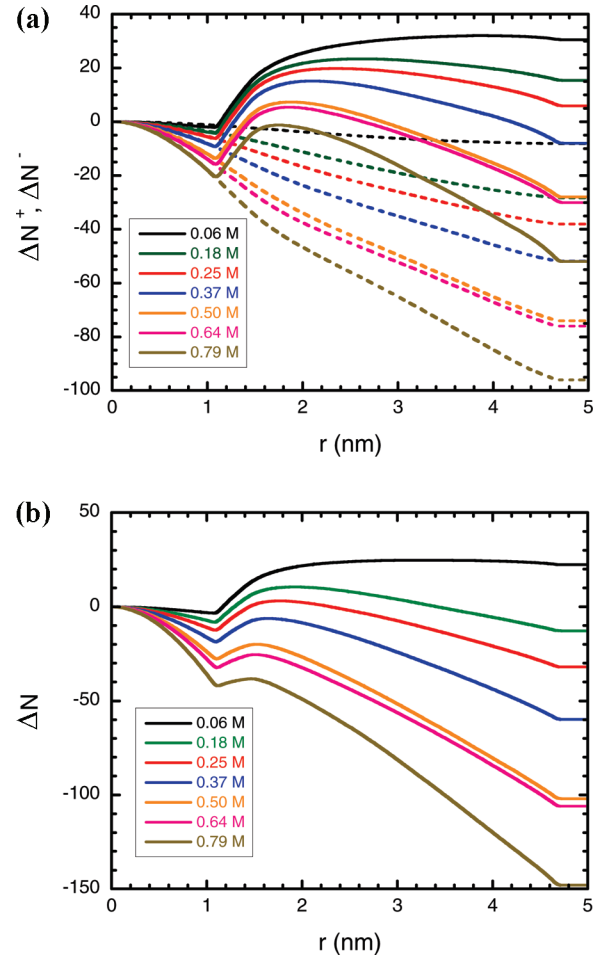

Figure 3. (a) The integrated excess number of ions versus radial distance in the DNA-blocked region relative to the buffer pore region. Solid lines: plus ion; dashed lines: minus ion. (b) The total integrated excess number of ions, i.e., the sum of plus and minus ions.

counterion peak near the DNA. The peak height, however, is concentration dependent, increasing with the ion concentration. To quantify counterion condensation to the DNA, we integrated the counterion distribution around the DNA in Figure 2a, obtained after subtracting the corresponding background distribution, represented by the plateau value of the counterion distribution in the same figure. This results in an integrated net excess number of counterions around the DNA. The background counterion distribution near the DNA can be thought of as the counterions that occupy the volume near the DNA other than the immediate vicinity of the charged sites. These are the counterions that are free and mobile and are not adsorbed to the DNA. The result is shown in Figure 4 where the excess number is expressed as a fraction of total charge on DNA (which is 50 in this study). We see that, for all the concentrations studied, the number of condensed counterions attains almost the same plateau value, about 0.60, at sufficiently large distance away from the DNA, with a small spread. Thus, we obtain here a net fraction of counterion condensation of about 60%. This value falls within the experimentally measured range of 0.53−0.85[15–20] but somewhat lower than the recent measured value of 0.75 using the optical tweezer technique[20] for the fractional counterion condensation.

On the basis of the electric neutrality, the fact that the experimentally measured counterion condensation fraction is smaller than unity suggests that the remaining counterions are distributed in the rest of the pore volume and contribute to the

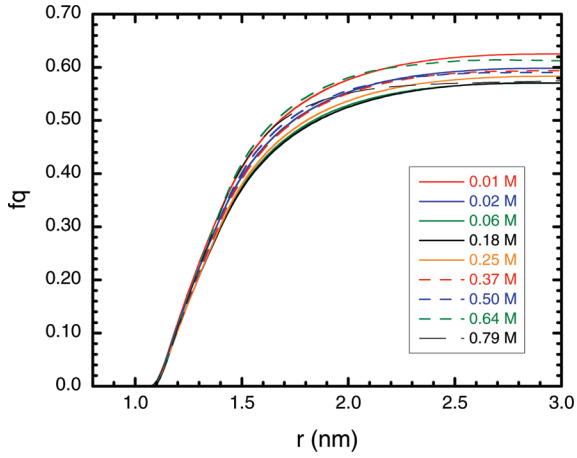

Figure 4. Excess number of counterions around the DNA as a fraction of charge on the DNA. This is obtained by subtracting the background contribution due to the concentration in the plateau region.

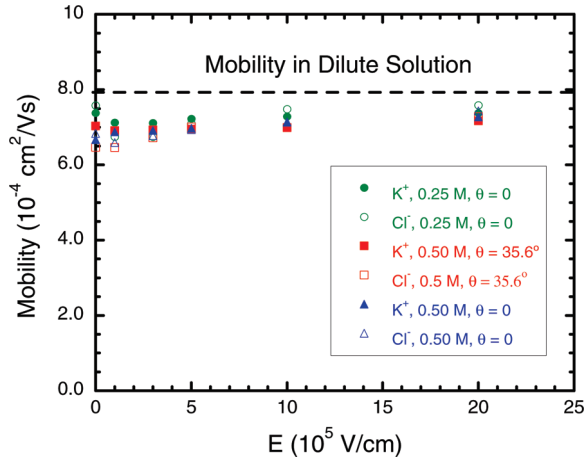

Figure 5. Mobility of ions for some typical cases. Solid symbols are for K^+, open symbols for Cl^-. DNA at center and parallel to the pore, ion concentration 0.25 M (circle); DNA at center and parallel to the pore, ion concentration 0.50 M (triangle); DNA tilted at 35.6° with pore axis, ion concentration 0.50 M (square). The dashed horizontal line corresponds to the mobility in bulk at infinite dilution limit.

background counterion distribution. Such background distribution can obviously lead to the difference in the plateau values in the ion distribution between the nanopore with and without the DNA.

III.4. Ion Mobility. We calculated ion mobility in the presence of DNA in the nanopore using both the equilibrium and nonequilibrium Brownian dynamics methods. In these calculations, the buffer pore portion as displayed in Figure 1 is removed, and the periodic boundary condition is used in the axial direction to simulate an infinitely long pore. In the equilibrium Brownian dynamics method, the mean square displacement is calculated, and the self-diffusion coefficient is derived from the Einstein relation, $\langle[\mathbf{r}_{\|}(t) - \mathbf{r}_{\|}(0)]^2\rangle = 2D_{\|}t$, applied only to the direction parallel to the axis of the nanopore. The mobility is determined through[31] $\mu = qD_{\|}/k_BT$. In the nonequilibrium method, the velocities of the ions are directly calculated from the simulation, and the mobility is derived through $\langle v\rangle/E$, where $\langle v\rangle$ is the time average of ion velocity, and E is the applied electric field; both are in the axial direction. The ion concentration obtained in the partition calculation for the DNA region was used for the mobility calculation. The mobility is calculated separately for the counterions and the co-ions. Note also that the mobility for counterions calculated here is an average over all counterions, including those counterions that are transiently adsorbed to the DNA.

The results are displayed for some typical ionic concentrations (close to the blockade current crossover concentration) in Figure 5. The values of mobility at the lowest field used in the calculations, 10^5 V/cm, and those derived form the self-diffusion coefficient are summarized in Table 4, together with those for the buffer pore. It is seen that the mobility obtained from the two methods agree with each other, consistent with fluctuation and dissipation theorem.[32–34] The ion mobility is generally lower than the corresponding mobility in bulk solution at infinite dilution: 7.62×10^{-4} cm^2/V s for K^+ and 7.91×10^{-4} cm^2/V s for Cl^-,[35] and slightly higher at low ion concentration, as expected. Also the difference between the mobility when the DNA is parallel to the pore axis and when the DNA is tilted with an angle is relatively small. Unlike in bulk solution, however, the co-ion mobility tends to be slightly lower than the counterions. This is probably due to the fact that the co-ions are the minority component and are thus more constrained in their movement when surrounded by the more numerous counterions. The mobility of ions in the DNA-blocked pore is slightly lower than that in the buffer pore. Part of the reason that the mobility obtained here is not more strongly affected in the DNA-blocked pore is that, at the relatively high and moderate ion concentration studied here, there exists in the pore a large proportion of free counterions (both to the DNA and to the wall) not adsorbed to the DNA, which can move freely without hindrance, giving rise to an apparent mobility not significantly reduced.

III.5. Blockade Current. In Figure 6 we show the blockade current calculated from the partition data and the ion mobility (Since the variation in mobility is small, for simplicity, we used the mobility obtained at ion concentration 0.50 M for all blockade current calculations. For DNA centered, we used the mobility value: 6.74×10^{-4} cm^2/V s; for DNA tilted, we used 6.69×10^{-4} cm^2/V s, which is the average of the counterion and co-ion nonequilibrium Brownian dynamics results at an electric field strength 10^5 V/cm in Table 4). The blockade current displayed corresponds to a 34 nm pore in length with a 120 mV voltage, similar to the experimental situation in the work of Smeets et al.[6] The four sets of data in the figure correspond to the following four cases: (1) DNA is centered at constant wall charge density (0.0276 C/m^2); (2) DNA is tilted with a 35.6° angle (which is the maximum tilting angle allowed for the length of DNA studied here) with respect to the pore axis at constant wall charge density as in (1); (3) DNA is centered and parallel to pore axis with a varying wall charge density (the wall charge density was varied using the formula given in the work of Heyden et al.[27,28]); and (4) the same as (2) but correcting the effect of the end-caps of the DNA. Clearly, the figure shows a trend of decreased blockade current with concentration, being positive at low ion concentration and negative at high ion concentration, reflecting the competition between volume exclusion (larger with increasing concentration), the counterion condensation to DNA, and the EDL overlap effect. The most obvious manifestation of EDL overlap effect is at low concentration, where the co-ions are strongly excluded due to the EDL overlap while the counterions are relatively more enriched. This leads to the co-ion concentration becoming negligible at significant bulk ion concentration. Our data suggest this already occurs at ion concentration 0.02 M or lower.

We recall that the DNA model used here has two semispherical caps at the ends, which are necessary to avoid mathematical singularity and to smoothly trace the dynamics of the ions during

TABLE 4: Self-Diffusion Coefficient and Mobility of Ions at Ion Concentrations of 0.25 and 0.50 M[a]

	K^+			Cl^-		
	buffer pore		DNA-blocked pore	buffer pore		DNA-blocked pore
conc. (M)	$D_{\|\|}$[b]	μ[c]	μ[c]	$D_{\|\|}$[b]	μ[c]	μ[c]
0.25	1.85	7.19	(7.35, 7.12)	1.89	7.34	(7.56, 6.75)
0.50[d]	1.83	7.11	(6.65, 6.88)	1.88	7.30	(6.82, 6.59)
0.50[e]	1.83	7.11	(7.01, 6.91)	1.88	7.30	(6.45, 6.46)

[a] For the DNA-blocked pore, the first number in the parentheses is mobility derived from self-diffusion coefficient, and the second number in the parentheses is the mobility obtained from non-equilibrium Brownian dynamic calculation. At a concentration of 0.50 M, the two rows of numbers are for the DNA parallel to the pore axis and tilted at 35.6° with respect to the pore axis. [b] Self-diffusion coefficient in the units of 10^{-5} cm^2/s. [c] Mobility in the units of 10^{-4} $cm^2/V \cdot s$. [d] DNA centered and parallel to the pore axis. [e] DNA is tilted at 35.6° with the pore axis.

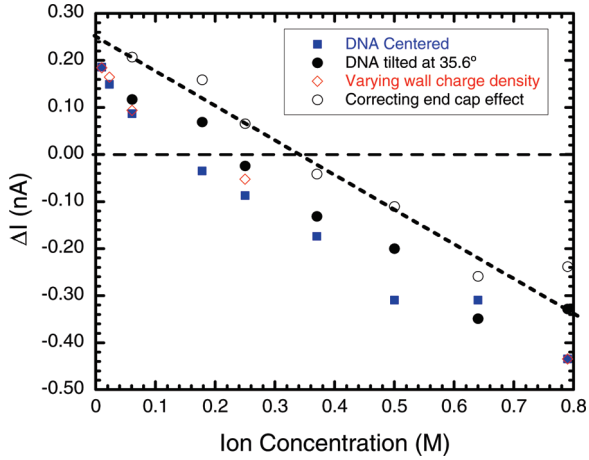

Figure 6. Blockade current through the nanopore at 3.53×10^4 V/cm: DNA centered and parallel to the pore axis without the DNA end-cap correction and at constant wall charge density (solid square); the same as above but with varying wall charge density (open diamond); DNA tilted with a 35.6° angle without the DNA end-cap correction, at constant wall charge density (solid circle); the same as above but with DNA end-cap correction (open circle).

the simulation. The cap portions of the DNA are without the embedded charge, the effect of which is to underestimate the counterion concentration in the DNA region while at the same time overestimating the counterion concentration in the buffer pore region. The open circles in Figure 6 represent the calculated blockade current taking into account the end-cap contribution for DNA tilted with a 35.6° angle with respect to the nanopore. On the basis of the cap radius of the DNA charge, we estimate a total of 13 additional embedded charges on DNA, with a net gain of 26 counterions in the DNA region relative to the open region. The open circles correspond to a simple shift up of the blockade current by 0.090 nA to correct this effect. Without the cap effect correction, the blockade current crosses zero at about 0.21 M (DNA centered) and 0.25 M (DNA tilted) at constant wall charge density, and about 0.22 M (DNA centered) for the varying wall charge. When the DNA cap effect is corrected, the crossover concentration increases to about 0.34 M, which is comparable to that of measured in experiment by Smeets et al., 0.37 M.[6]

Comparison between DNA centered and DNA tilted cases shows that the DNA segment with a tilting angle increases the blockade current. In addition, it also shows that simply placing the DNA at the center parallel to the nanopore produces a reasonably close estimate for the blockade current crossover concentration. Our calculations suggest that most of the effect of the tilted DNA is essentially to increase the number of charges for the longer segment of DNA when positioned with a tilting angle with respect to the pore axis, and hence the counterions.

It is noted that a simple analysis based on the volume exclusion and counterion condensation provided a prediction in reasonable accord with experiment without considering the EDL overlap effect. This may be partly due to the fact that, by assuming the same concentration in the DNA region and the bulk, the simple theory may somewhat overestimate the volume exclusion of the co-ions, thus partly accounting for the EDL overlap effect.

We also note here that Fan et al. observed a blockade current crossover at a higher concentration in a 50 nm pore.[5] This shift to higher crossover concentration for larger pore should be expected. The main reason is the negligible effect for EDL overlap for such large pore at relatively high ionic concentration. Since the EDL overlap effect on blockade current is negative, for larger pores, the crossover concentration shifts to higher value. This suggests that the blockade current crossover concentration should be nanopore size dependent.

The effect of wall charge on the blockade current crossover seems relatively minor in the range of ion concentration and wall charge density studied here (at the highest ion concentration, 0.79 M, we have used the same wall charge density for both constant and varying wall charge density cases). As shown in Figure 6, the difference is statistically insignificant. The effect of wall charge density would probably become more apparent at lower ion concentration where the co-ions are completely excluded. By electric neutrality, and since the amount of charge on DNA is fixed, the variation of the total number of conducting ions (counterions) and thus the current are completely determined by the wall charge, as found in the work of Smeets et al.[6]

IV. Conclusions

We have carried out a detailed Brownian dynamics simulation study of ionic current blockade due to the presence of DNA in nanopores. Our results confirm the recent experimental results by a number of recent studies. In addition to the volume exclusion and the counterion condensation mechanisms suggested by previous studies, we also find that the EDL overlap plays a significant role. The introduction of a DNA carrying densely populated charges into the nanopore immediately reduces the distance between fixed charges (on the wall and on the DNA) by more than half, causing EDL overlap to commence at a higher ionic concentration. One manifestation of this effect is the split of the counterion and co-ion density distribution profiles with increasing gap size as ion concentration decreases. At sufficiently low ionic concentration, the co-ions are completely excluded, leaving only counterions in the pore. Then the total amount of counterions equals the sum of the wall charges plus the DNA charges. As the DNA charges are only partially compensated by the Manning condensation (with a fractional condensation factor always less than unity), the

remaining counterions form the background ions distributed throughout the nanopore and are therefore mobile. The counterions adsorbed to the DNA, especially the monovalent ions, have a limited lifetime and can dissociate and frequently exchange roles with the mobile ions. The availability of the mobile ions when the adsorbed ions dissociate significantly affects the counterion condensation equilibrium, which may explain the counterion distribution peak decrease with ion concentration.

Our study of the ion mobility suggests that the presence of DNA tends to reduce the ion mobility. Such reduction would become more important at low ion concentration with low charge density on the pore where there are few mobile ions. In addition, we observe that, in the buffer pore, the Cl^- tends to have a slightly higher mobility than K^+ consistent with bulk behavior. In the presence of DNA, however, the Cl^- seems to have a slightly lower mobility, possibly due to the restrictive effect imposed by the EDL, reducing the available routes for the co-ions to complete a displacement.

Our investigation of the counterion condensation onto DNA for 2 orders of magnitude in ionic concentration showed little variation in the fraction of excess counterions over the amount of charges carried by the DNA. We obtain a fraction of about 0.6, within the range of the experimental values.

The blockade current and its crossover concentration are affected by several factors. In addition to the volume exclusion and counterion condensation, the EDL overlap plays an important role. DNA conformation also contributes significantly to blockade current and the crossover concentration, becoming more important at low concentration. Both of which could lead to pore size dependence of the blockade current and its crossover concentration.

Acknowledgment. The work is supported by a grant from the NIH under the Contract Number R01 HG002647-03. The author would like to thank Dr. J. M Ramsey and his group for many useful discussions during the course of this work.

References and Notes

(1) Kasianowicz, J. J.; Brandin, E.; Branton, D.; Deamer, D. W. *Proc. Natl. Acad. Sci. U.S.A.* **1996**, *93*, 13770.

(2) Song, L. Z.; Hobaugh, M. R.; Shustak, C.; Cheley, S.; Bayley, H.; Gouaux, J. E. *Science* **1996**, *274*, 1859.

(3) Akeson, M.; Branton, D.; Kasianowicz, J. J.; Brandin, E.; Deamer, D. W. *Biophys. J.* **1999**, *77*, 3227.

(4) Meller, A.; Nivon, L.; Brandin, E.; Golovchenko, J.; Branton, D. *Proc. Natl. Acad. Sci.* **2000**, *97*, 1079.

(5) Fan, R.; Karnik, R.; Yue, M.; Li, D.; Majumdar, A.; Yang, P. *Nano Lett.* **2005**, *5*, 1633.

(6) Smeets, R. M. M.; Keyser, U. F.; Krapf, D.; Wu, M.-Y.; Dekker, N. H.; Dekker, C. *Nano Lett.* **2006**, *6*, 89.

(7) Liang, X.; Chou, S. Y. *Nano Lett.* **2008**, *8*, 1472.

(8) Chang, H.; Kosari, F.; Andreadakis, G.; Alam, M. A.; Vasmatzis, G.; Bashir, R. *Nano Lett.* **2004**, *4*, 1551.

(9) Menard, L.; Mair, C.; Ramsey, J. M., Department of Chemistry, University of North Carolina at Chapel Hill, Chapel Hill, NC 27599-3216. To be submitted for publication.

(10) Adamson A. W.; Gast, A. P. *Physical Chemistry of Surfaces*, 6th ed.; John Wiley and Sons: New York, 1997.

(11) Hunter, R. J. *Foundations of Colloid Science*; Clarendon Press: Oxford, 1987.

(12) Cui, S. T. *Phys. Rev. Lett.* **2007**, *98*, 138101.

(13) Reisner, W.; Morton, K. J.; Riehn, R.; Wang, Y. M.; Yu, Z.; Rosen, M.; Sturm, J. C.; Chou, S. Y.; Frey, E.; Austin, R. H. *Phys. Rev. Lett.* **2005**, *94*, 196101.

(14) Odijk, T. *Macromolecules* **1983**, *16*, 1340.

(15) Manning, G. S. *Q. Rev. Biophys.* **1978**, *11*, 179.

(16) Jayaram, B.; Beveridge, D. L. *Annu. Rev. Biophys. Biomol. Struct.* **1996**, *25*, 367.

(17) Padmanabhan, S.; Richey, B.; Anderson, C. F.; Record, J. M. T. *Biochemistry* **1988**, *27*, 4367.

(18) Schellman, J. A.; Stigter, D. *Biopolymers* **1977**, *16*, 1415.

(19) Stellwagen, E.; Stellwagen, N. C. *Biophys. J.* **2003**, *84*, 1855.

(20) Keyser, U. F.; Koeleman, B. N.; Krapf, D.; Smeets, R. M. M.; Lemay, S. G.; Dekker, N. H.; Dekker, C. *Nat. Phys.* **2006**, *2*, 473.

(21) Ermak, D. L. *J. Chem. Phys.* **1975**, *62*, 4189.

(22) Ermak, D. L. *J. Chem. Phys.* **1975**, *62*, 4197.

(23) Allen M. P.; Tildesley, D. J. *Computer Simulation of Liquids*; Oxford University Press: Oxford, 1987.

(24) Montoro, J. C. G.; Abascal, J. L. F. *J. Chem. Phys.* **1995**, *103*, 8273.

(25) Dang, L. X.; Kollman, P. A. *J. Phys. Chem.* **1995**, *99*, 55.

(26) See for example Arcesi, L.; La Penna, G.; Perico, A. *Biopolymer* **2007**, *86*, 127. Schiessel, H. *J. Phys.: Condens. Matter* **2003**, *15*, R699, and references therein.

(27) Van der Heyden, F. H. J.; Stein, D.; Dekker, C. *Phys. Rev. Lett.* **2005**, *95*, 116104.

(28) We have used the prescription in ref 27 to obtain the surface charge density at varying ionic concentration by solving eqs 5 and 6 of ref 27 iteratively. The parameters we used are those suggested in citation 18 of ref 27: $\Gamma = 8\ nm^{-2}$, $pK = 7.9$, $pH = 8.0$, and $C = 0.3\ Fm^{-2}$, $T = 25°\ C$, $\varepsilon = 78.4$.

(29) Cui, S. T. *J. Chem. Phys.* **2005**, *123*, 054706.

(30) Boda, D.; Busath, D. D.; Henderson, D.; Sokolowski, S. *J. Phys. Chem. B* **2000**, *104*, 8903.

(31) Lee, S. H.; Rasaiah, J. C. *J. Chem. Phys.* **1996**, *100*, 1420.

(32) Onsager, L. *Phys. Rev.* **1931**, *37*, 405. Onsager, L. *Phys. Rev.* **1931**, *38*, 2265.

(33) Green, M. S. *J. Chem. Phys.* **1954**, *22*, 398.

(34) Kubo, R. *J. Phys. Soc. Jpn.* **1957**, *12*, 570.

(35) Lide, D. R. *CRC Handbook of Chemistry and Physics*, 89th ed.; CRC Press: Boca Raton, FL, 2008−2009. Online at http://www.hbcpnetbase.com/.

JP909564D